J. Iron Steel Res. Int. (2022) 29:327–338
https://doi.org/10.1007/s42243-021-00606-1

ORIGINAL PAPER

Evolution of microstructure in reheated coarse-grained zone of G115 novel martensitic heat-resistant steel

Zhong-yi Chen[1] · Zheng-zong Chen[2] · Dong-xu Kou[1] · Yong-qing Li[3] · Yong-lin Ma[1] · Yi-ming Li[4]

Received: 4 December 2020 / Revised: 8 March 2021 / Accepted: 9 March 2021 / Published online: 17 May 2021

Abstract
Based on the thermal simulation method, a systematical analysis was conducted on the effect of welding peak temperature and the cooling time that takes place from 800 to 500 °C on microstructure, precipitates, substructure and microhardness of the reheated coarse-grained heat-affected zone (CGHAZ) of G115 novel martensitic heat-resistant steel. As revealed from the results, the microstructure of un-altered CGHAZ (UACGHAZ) and supercritically CGHAZ (SCCGHAZ) was lath martensite, and structural heredity occurred. Intercritically reheated CGHAZ (IRCGHAZ) exhibited martensite and over-tempered martensite, and subcritical CGHAZ (SCGHAZ) displayed martensite and under-tempered martensite. The austenite in UACGHAZ and SCCGHAZ was transformed with the diffusion mechanism during the first thermal cycle, but with the non-diffusion mechanism during the second thermal cycle. For this reason, A_{c1} and A_{c3} during the second thermal cycle were significantly lower than those during the first thermal cycle, and A_{c1} and A_{c3} were reduced by nearly 14 and 44 °C, respectively. Since the content and stability of the austenite alloy during the second thermal cycle of IRCGHAZ were lower than those during the first thermal cycle, M_s increased by nearly 30 °C. There were considerable precipitates in the over-tempered region of IRCGHAZ, and the Laves phase was contained, which was not conducive to high-temperature creep property. Moreover, the dislocation density and the number of sub-grains in the region were lower, resulting in a sharp decrease in the microhardness, and it was the weak area in the reheated CGHAZ.

Keywords Heat-resistant steel · G115 steel · Reheated coarse-grained heat-affected zone · Microstructure evolution · Precipitate

1 Introduction

In the 600 °C ultra-supercritical steam generator set, the large diameter pipe of the high-temperature section is primarily made from P92 steel, with the upper limit of service temperature of 628 °C [1, 2]. Improving the steam parameter can increase the generating efficiency of the unit, as well as reduce the coal consumption and CO_2 emission. The existing heat-resistant steel for 700 °C ultra-supercritical generator set has been developed in European and American nations [3]. The G115 steel (9Cr–3W–3Co–1CuVNbB) refers to a novel generation of heat-resistant steel developed by China Iron & Steel Research Institute Group (CISRI). Its high-temperature creep strength and rupture strength are significantly better than those of the P92 steel [4–9]. Overall, the heat-affected zone (HAZ) of welding acts as the weak area of the heat-resistant steel in service. The type IV failure of conventional P91 and P92 steels during the service period shows a close relation to the HAZ microstructure, grain size, the precipitate as well as substructure evolution [10, 11]. In the study on the HAZ structure and properties of the P92 steel, Abe et al. [10] reported that the stress state, grain size, non-uniform

✉ Zhong-yi Chen
czychenzhongyi@imust.cn

[1] School of Material and Metallurgy, Inner Mongolia University of Science and Technology, Baotou 014010, Inner Mongolia, China

[2] Institute for Special Steels, China Iron and Steel Research Institute, Beijing 100081, China

[3] Technology Center, Inner Mongolia North Heavy Industry Group Co., Ltd., Baotou 014010, Inner Mongolia, China

[4] Key Laboratory of Advanced Metals and Materials of Inner Mongolia of Materials and Metallurgy School, Inner Mongolia University of Science and Technology, Baotou 014010, Inner Mongolia, China

distribution of carbides and formation of coarse Laves phase in the fine-grained HAZ were the major causes of type IV failure of the material. Matsunaga et al. [12] and Abstoss et al. [13] determined the welding joint structure and properties of the 9Cr–3W–3Co–VNb steel and the MarBN steel. To be specific, they suggested that the HAZ of this type of heat-resistant steel remains the zone where failure is easy to occur during the service period.

During the multi-pass welding of the thick plate or the thick wall material, the phase transformation and microstructure evolution of the reheated coarse-grained heat-affected zone (CGHAZ) are the major factors influencing the material properties. For the materials exhibiting strong hardenability, the structural heredity is easy to occur in the un-altered CGHAZ (UACGHAZ) and supercritically CGHAZ (SCCGHAZ) under the memory effect of austenite, thereby leading to the coarsening of original austenite grains, an increase in brittleness and a decrease in toughness. In the study on the microstructure and properties of the HAZ of multi-pass welding of the S355 steel and the 10CrNi3-MoV steel, Gao et al. [14] and Peng et al. [15] revealed that the original austenite grain size of UACGHAZ and SCCGHAZ complied with that of CGHAZ causes a sharp decrease in toughness. In the intercritically reheated CGHAZ (IRCGHAZ), the properties of the material decrease significantly due to the existence of mixed structure with obvious difference in structure types and properties. When studying the microstructure and properties of the reheated CGHAZ of the X65 and X80 steels, Arora et al. [16] found that the toughness of IRCGHAZ decreased as impacted by the coarsening of IRCGHAZ grains and martensite-austenite (M-A) components. In the study on the microstructure and properties of the reheated CGHAZ of the WB36 steel, Wang et al. [17, 18] reported that the embrittlement of IRCGHAZ was attributed to the strip-shaped M-A component existing in the grain, and the postweld heat treatment could decompose most of the strip-shaped M-A components, as an attempt to enhance its toughness. In the analysis of the reheated CGHAZ of the P92 steel, Xu et al. [19] indicated that the IRCGHAZ of the P92 steel contained fine structure and undissolved carbides, and the microhardness decreased under the coarsening of carbides in the subcritical CGHAZ (SCGHAZ). Likewise, the phase transformation, microstructure, precipitate, substructure and microhardness of the reheated CGHAZ of the G115 steel will affect the material performance in the service phase. To reveal the evolution law of the microstructure and properties of the reheated CGHAZ of the G115 steel, the reheated CGHAZ at different peak temperatures and under different heat inputs was tested by adopting the thermal simulation method on the Gleeble-1500D thermal simulator. The microstructure, grain size, precipitate and substructure of the reheated CGHAZ were observed and analyzed under the scanning electron microscope (SEM) and the transmission electron microscope (TEM), and the microhardness was measured and analyzed subsequently.

2 Experimental material and method

The experimental material was the G115 steel pipe provided by CISRI with the external diameter of 60 mm and the wall thickness of 10 mm, whose chemical composition is as follows (in wt.%): C 0.097, Si 0.31, Mn 0.43, Cr 9.11, Co 2.98, W 2.67, V 0.18, Nb 0.066, Cu 0.85, B 0.013, N 0.008 and Fe balance. The heat treatment was normalizing at 1080 °C for 1.5 h (air cooling) and tempering at 775 °C for 3 h (air cooling). The thermodynamic calculation of equilibrium phase was conducted by Thermal-Calc. The size of thermal simulation sample was ϕ6 mm × 105.5 mm. The heating rate of welding thermal simulation was 200 °C/s, and it stayed at the peak temperature (T_p) for 1 s. The welding thermal simulation sample underwent two thermal cycles. To be specific, during the first thermal cycle, T_{p1} was 1350 °C, and the welding cooling time that takes place from 800 to 500 °C ($t_{8/5}$) was 25 s, which was used to obtain the CGHAZ. Next, the reheated CGHAZ under different T_{p2} and $t_{8/5}$ was obtained for the second time based on the first thermal cycle. During the second thermal cycle, the T_{p2} was 1350, 1150, 900 and 770 °C, respectively, and the corresponding reheated CGHAZ was UACGHAZ, SCCGHAZ, IRCGHAZ and SCGHAZ, respectively. Moreover, there were three $t_{8/5}$ under each T_{p2}, i.e., 25, 50 and 150 s, respectively. The sample undergoes two welding thermal cycles and is replaced by "$t_{8/5}$ = 25 s–25 s", which means that the first thermal cycle $t_{8/5}$ is 25 s and the second thermal cycle $t_{8/5}$ is 25 s. The welding thermal simulation parameters are listed in Table 1. According to the thermal dilatation curve, A_{c1}, A_{c3}, M_s and M_f under different conditions were obtained. The polished surface of the sample was etched with $FeCl_3$ (10 g), HCl (30 mL) and H_2O (160 mL) for 30 s, and the microstructure was observed under the SEM (Super55). The films were formed by double-jet electropolishing in 150 mL $HClO_4$ and 850 mL CH_3-CH_2OH solution at 25 °C and 30 V, and the microstructure and the precipitate were observed with TEM (JEM-2100). The microhardness of the sample was measured with the Vickers hardness tester (W-20).

3 Results

3.1 Microstructure of base metal

Figure 1 illustrates the microstructure of the G115 steel base metal. The microstructure of G115 steel base metal is characterized by typical tempered martensite structure

Table 1 Welding thermal simulation schemes of G115 steel

Position	First-pass holding temperature T_{p1}/°C	First pass $t_{8/5}$/s	Second-pass heating rate v/(°C s^{-1})	Second-pass holding temperature T_{p2}/°C	Second pass $t_{8/5}$/s
UACGHAZ	1350	25	200	1350	25, 50, 150
SCCGHAZ	1350	25	200	1150	25, 50, 150
IRCGHAZ	1350	25	200	900	25, 50, 150
SCGHAZ	1350	25	200	770	25, 50, 150

(Fig. 1a), exhibiting obvious lath-shaped distribution inside the grain. Besides, there are considerable precipitates in the grain boundary, the lath boundary and the grain. The excellent properties of G115 steel are the comprehensive embodiment of solution strengthening, grain refinement strengthening, dislocation strengthening and precipitation strengthening. To be specific, the precipitation strengthening is critical to ensure that the material exhibits excellent high-temperature creep strength [1, 8, 12]. The main precipitates in G115 steel were Cr/Fe/W-rich carboborite $(Cr,Fe,W)_{23}(C,B)_6$ and Nb/V-rich carbonitride (Nb,V)(C,N). Figure 1b indicates that $(Cr,Fe,W)_{23}(C,B)_6$ displayed the face-centered cubic (FCC) structure, primarily round or oval and largely distributed in the original austenite grain boundary, lath boundary and block boundary, exhibiting a diameter of 100–200 nm. In addition, (Nb,V)(C,N) displayed the FCC structure, mostly regular quadrilateral or circular and mainly distributed in the original austenite grain, achieving a diameter of 40–60 nm. The mentioned two precipitates refer to the main strengthening phases in the G115 steel, capable of pinning the grain boundaries and free dislocations, as an attempt to ensure long-term stability of the microstructure at high temperatures. W/Cr/Fe-rich Laves phase $(Fe,Cr)_2W$ [1, 2, 8, 12], W/Cr/Fe-rich μ phase $(Fe,Cr)_7W_6$ [20] and Cu-rich phase [8] will be formed on the matrix after welding, aging or service. To be specific, the copper-rich phase will form and significantly stabilize the microstructure at the early stage of service, and the formation of Laves phase often means to the beginning of the decline of high-temperature creep properties.

3.2 Dilatometric curve and microstructure of UACGHAZ

Figure 2 plots the thermal dilatation curves of UACGHAZ. Figure 2a illustrates the thermal dilatation curves of two thermal cycles when $t_{8/5}$ = 25 s–25 s, and Fig. 2b shows the local thermal dilatation curves of the second thermal cycle during the cooling under different $t_{8/5}$. Figure 2a indicates that during the first thermal cycle, the tempered martensite ($M_{Tempered}$) of the base metal was completely transformed into the austenite (γ_{First}) and then into the martensite (M_{First}) during the cooling. During the second thermal cycle, the transformed product martensite (M_{First}) of the first thermal cycle was transformed into the austenite (γ_{Second}) and subsequently into martensite (M_{Second}) again during the cooling. Since the phase-transformed products of the two thermal cycles in this region are martensite, and the grain size is unchanged, it is termed as UACGHAZ,

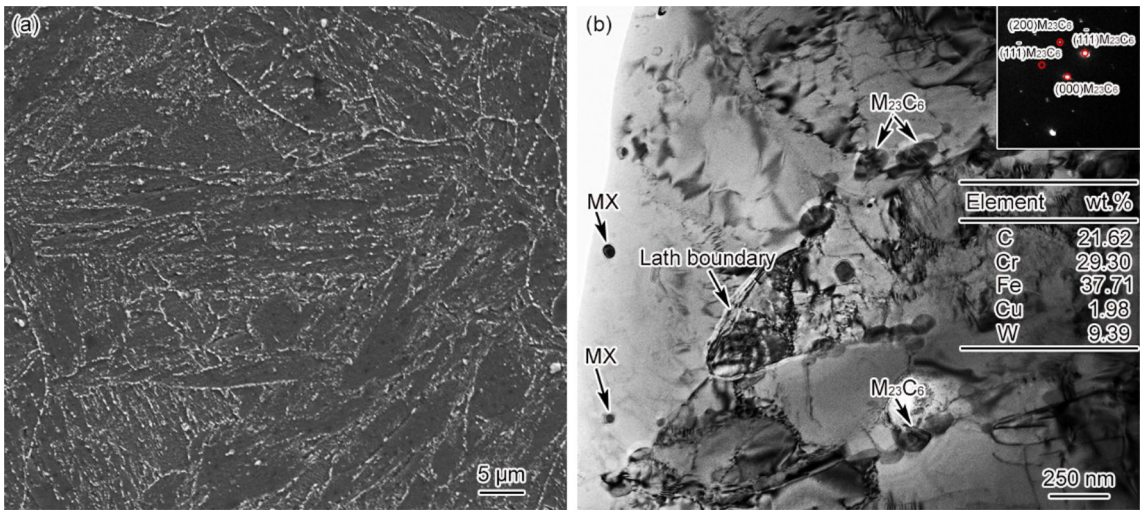

Fig. 1 Microstructure of base metal. **a** SEM; **b** TEM

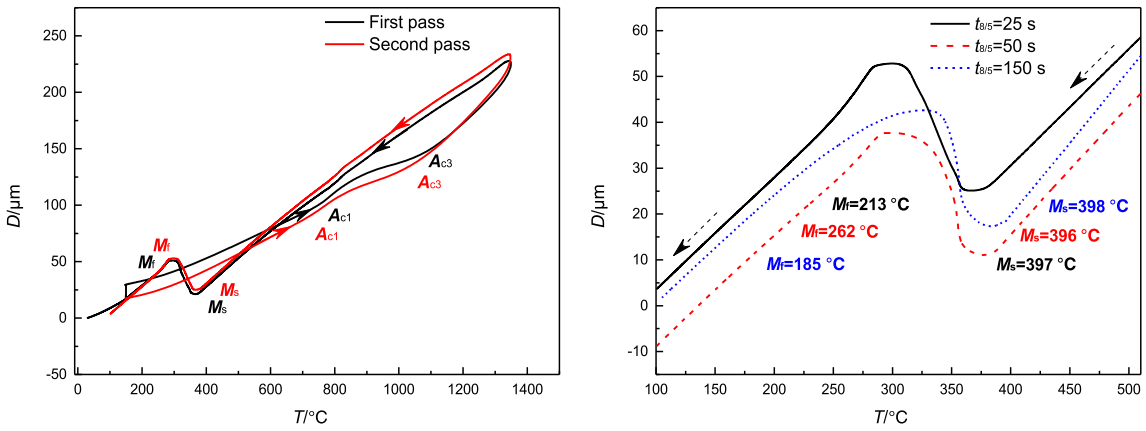

Fig. 2 Dilatation curves in UACGHAZ. **a** $t_{8/5}$ = 25 s–25 s; **b** cooling

i.e., the structural heredity [14, 15]. According to Fig. 2b, when $t_{8/5}$ of the second thermal cycle was 25, 50 and 150 s, M_s was 397, 396 and 398 °C, and M_f was 213, 262 and 185 °C, respectively. Welding $t_{8/5}$ slightly impacted the martensitic transformation point of UACGHAZ. Moreover, the M_s and M_f in the first and the second thermal cycles were consistent. A_{c1} and A_{c3} during the first thermal cycle were 821 and 1131 °C, respectively, and A_{c1} and A_{c3} during the second thermal cycle were 807 and 1087 °C, respectively, and the austenite transformation temperature was down-regulated significantly. Figure 3 presents the microstructure of UACGHAZ at $t_{8/5}$ = 25 s–25 s. The microstructure of UACGHAZ was coarse lath martensite exhibiting clear lath boundary, which contained considerable dislocation tangles and sub-grains, as well as a small amount of lamellar residual austenite between martensite laths (Fig. 3b). When $t_{8/5}$ increased from 25 to 150 s, the average grain size increased from 54 to 67 μm. The grain size of UACGHAZ increased with the increasing $t_{8/5}$.

Combined with Figs. 2 and 3, the phase transformation law of UACGHAZ of G115 steel is written as:

$$M_{Tempered} \xrightarrow{heating} \gamma_{First} \xrightarrow{cooling} M_{First} \xrightarrow{heating} \gamma_{Second} \xrightarrow{cooling} M_{Second}.$$

3.3 Dilatometric curve and microstructure of SCCGHAZ

The SCCGHAZ thermal dilatation curves are plotted in Fig. 4. Figure 4a shows that except for the second thermal cycle T_{p2}, the varying trends of thermal dilatation curves of SCCGHAZ and UACGHAZ were basically the same, the martensitic transformation occurred in both thermal cycles, and the structural heredity was identified. As suggested in Fig. 4b, $t_{8/5}$ of the second thermal cycle was 25, 50 and 150 s, and the corresponding M_s was 383, 396 and 397 °C, and M_f was 256, 262 and 200 °C, respectively. M_s and M_f of SCCGHAZ and UACGHAZ were consistent. Figure 5

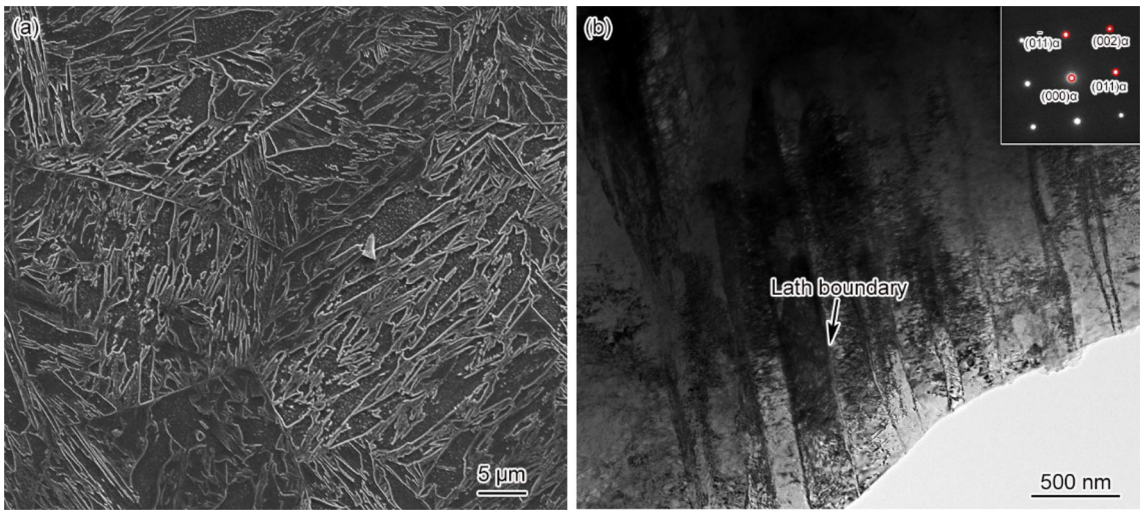

Fig. 3 Microstructure of UACGHAZ, $t_{8/5}$ = 25 s–25 s. **a** SEM; **b** TEM

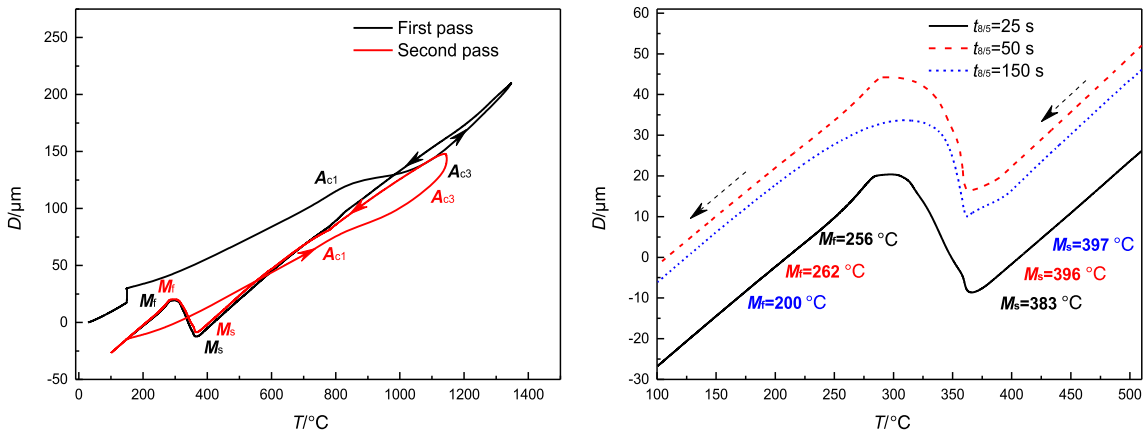

Fig. 4 Dilatation curves in SCCGHAZ. **a** $t_{8/5}$ = 25 s–25 s; **b** cooling

illustrates the microstructure of SCCGHAZ when $t_{8/5}$ = 25 s–25 s. The microstructure of SCCGHAZ was lath martensite exhibiting clear lath boundaries. The grain size, lath width, dislocation density and number of sub-grains were reduced as compared with those of UACGHAZ (Fig. 5b). When $t_{8/5}$ increased from 25 to 150 s, the average grain size increased from 54 to 61 μm. A small quantity of undissolved carbides exhibiting the size of 40–60 nm were found between the martensite laths using the TEM (Fig. 5b), while no undissolved carbides were identified in UACGHAZ, demonstrating that the variation of T_{p2} will affect the dissolution behavior of carbides. It was suggested that most of the undissolved carbides were $(Cr,Fe,W)_{23}C_6$ carbides (Fig. 6).

Combined with Figs. 4 and 5, the phase transformation law of SCCGHAZ of G115 steel is written as:

$$M_{Tempered} \xrightarrow{heating} \gamma_{First} \xrightarrow{cooling} M_{First} \xrightarrow{heating} \gamma_{Second} \xrightarrow{cooling} M_{Second}.$$

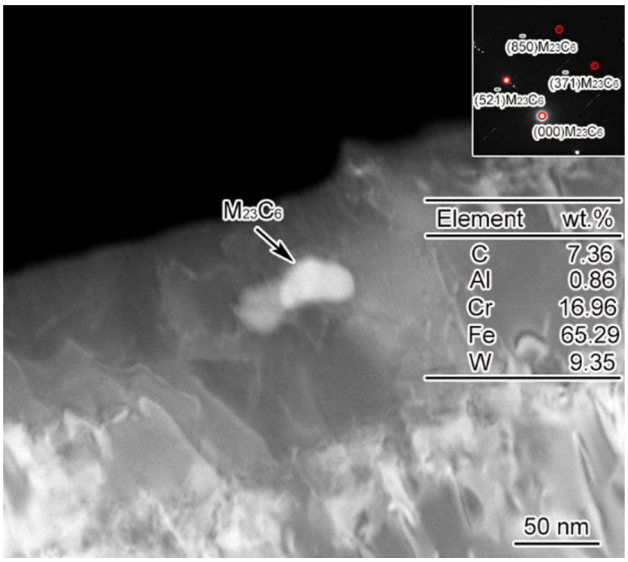

Fig. 6 Undissolved carbides in SCCGHAZ

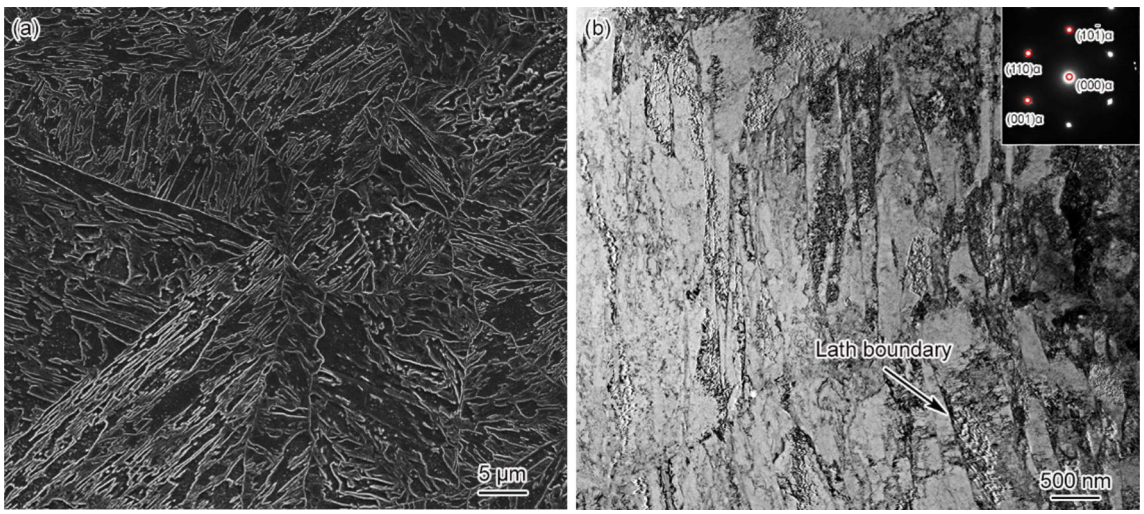

Fig. 5 Microstructure of SCCGHAZ, $t_{8/5}$ = 25 s–25 s. **a** SEM; **b** TEM

3.4 Dilatometric curve and microstructure of IRCGHAZ

Figure 7 plots the thermal dilatation curve of IRCGHAZ. As shown in Fig. 7a, T_{p2} during the second thermal cycle of IRCGHAZ ranged from A_{c1} to A_{c3}, and the martensite was partially transformed into austenite and subsequently transformed into martensite during the cooling, while the untransformed part led to the formation of the over-tempered martensite during the thermal cycling [16] and remained during the cooling. According to Fig. 7b, when $t_{8/5}$ of the second thermal cycle was 25, 50 and 150 s, the corresponding M_s reached 395, 415 and 432 °C, and M_f was 233, 242 and 213 °C, respectively. The M_s of IRCGHAZ increased with the increase in $t_{8/5}$. Moreover, when $t_{8/5}$ = 150 s, the M_s of IRCGHAZ increased by nearly 30 °C in comparison with UACGHAZ and SCCGHAZ, suggesting that the austenite chemical composition and stability of IRCGHAZ during the second thermal cycle were significantly different from those of UACGHAZ and SCCGHAZ.

The microstructure of IRCGHAZ at $t_{8/5}$ = 25 s–25 s is illustrated in Fig. 8. According to Fig. 8a, the microstructure of IRCGHAZ was a mixture of martensite and over-tempered martensite ($M_{Over\text{-}tempered}$). Figure 8b indicates that in the martensite region, the lath boundaries were clear, and numerous dislocation tangles and sub-grains existed in the lath, with a small quantity of undissolved carbides; the over-tempered martensite region exhibited the fuzzy lath boundaries and the sharply decreasing dislocation density and number of sub-grains, as well as considerable undissolved carbides. As revealed from the further observation on the undissolved carbides in the over-tempered martensite region, most of the undissolved carbides were elliptical, exhibiting the size of 60–120 nm, and significantly larger than SCCGHAZ. The carbide interface maintained a certain orientation relationship with the matrix, as shown in Fig. 9a. As revealed from the analysis of the energy-dispersive spectrometer (EDS) energy spectrum and the diffraction pattern, the carbide was $M_{23}C_6$ rich in Fe, Cr and W. Moreover, there was a small quantity of W-rich precipitate around the chain-like undissolved $M_{23}C_6$ carbide. Such precipitate displayed irregular block distribution, exhibiting the size of 220–290 nm (Fig. 9b). According to the EDS spectrum and the diffraction pattern, the precipitate was Laves phase rich in W, Fe and Cr.

According to Figs. 7 and 8, the phase transformation law of IRCGHAZ of G115 steel is expressed as:

$$M_{Tempered} \xrightarrow{heating} \gamma_{First} \xrightarrow{cooling} M_{First} \xrightarrow{heating} \gamma_{Second} + M_{Over-tempered} \xrightarrow{cooling} M_{Second} + M_{Over-tempered}.$$

3.5 Dilatometric curve and microstructure of SCGHAZ

The SCGHAZ thermal dilatation curves are plotted in Fig. 10, which shows that T_{p2} of SCGHAZ during the second thermal cycle was lower than A_{c1}, no austenite transformation was identified, and no new phase was formed. However, part of the martensite might be tempered incompletely or at low temperatures during the secondary thermal cycle, thereby leading to the formation of the under-tempered martensite ($M_{Under\text{-}tempered}$). Figure 11 illustrates the microstructure of SCGHAZ at $t_{8/5}$ = 25 s–25 s. The microstructure of SCGHAZ was a mixture of lath martensite and under-tempered martensite. As observed under the SEM, the martensite was gray with considerable lath structure, and the under-tempered martensite was dark gray exhibiting fuzzy lath boundary (Fig. 11a). TEM shows that revival occurred in the region of under-tempered martensite, and the dislocation density and the number of sub-grains decreased, while the lath boundary in

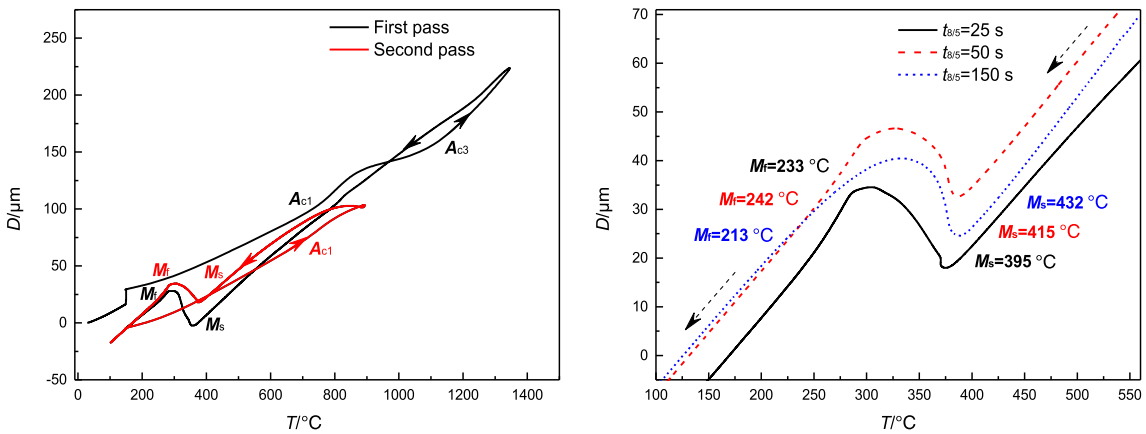

Fig. 7 Dilatation curves in IRCGHAZ. **a** $t_{8/5}$ = 25 s–25 s; **b** cooling

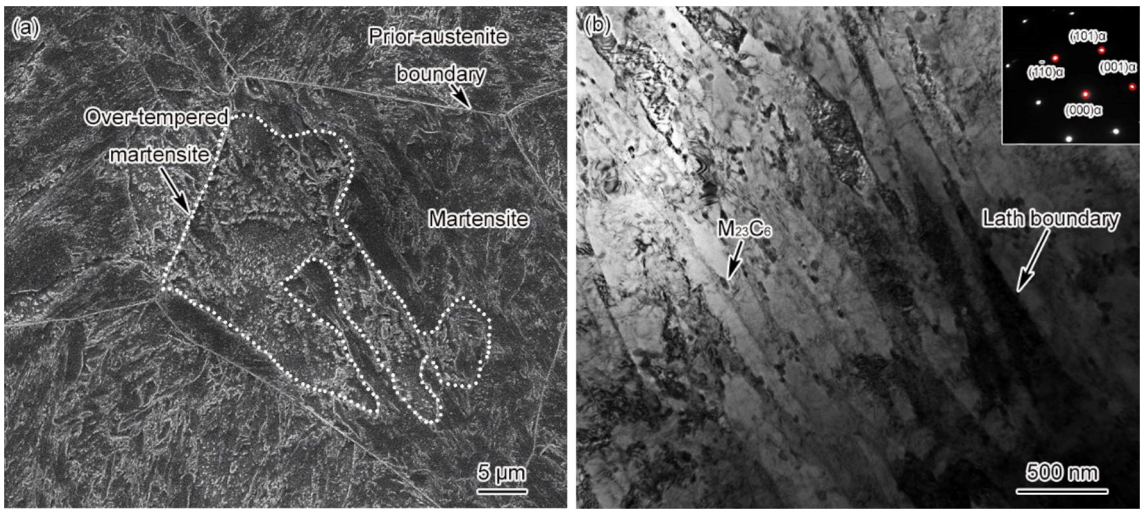

Fig. 8 Microstructure of IRCGHAZ, $t_{8/5}$ = 25 s–25 s. **a** SEM; **b** TEM

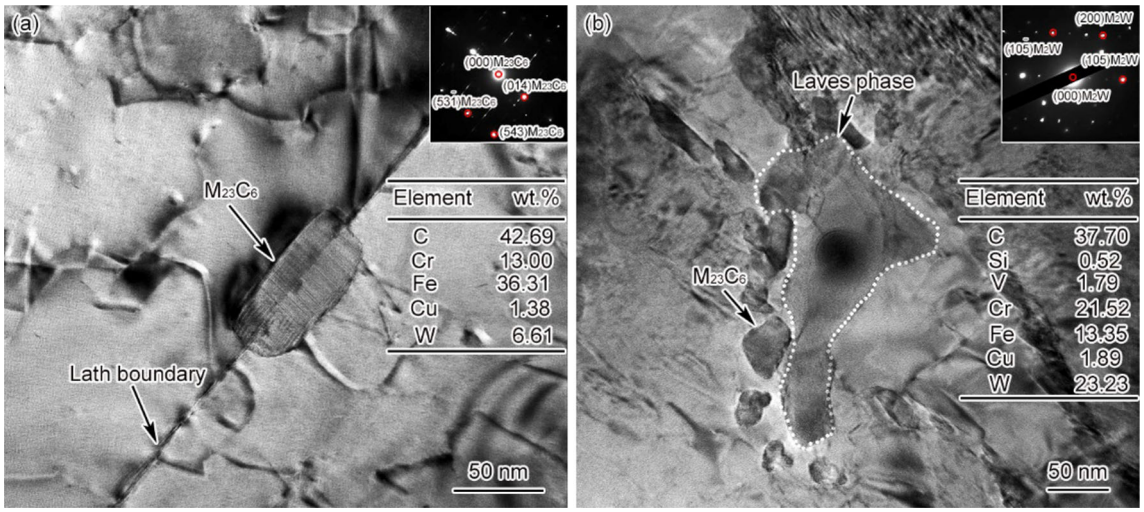

Fig. 9 Precipitations in IRCGHAZ. **a** $M_{23}C_6$; **b** Laves phase

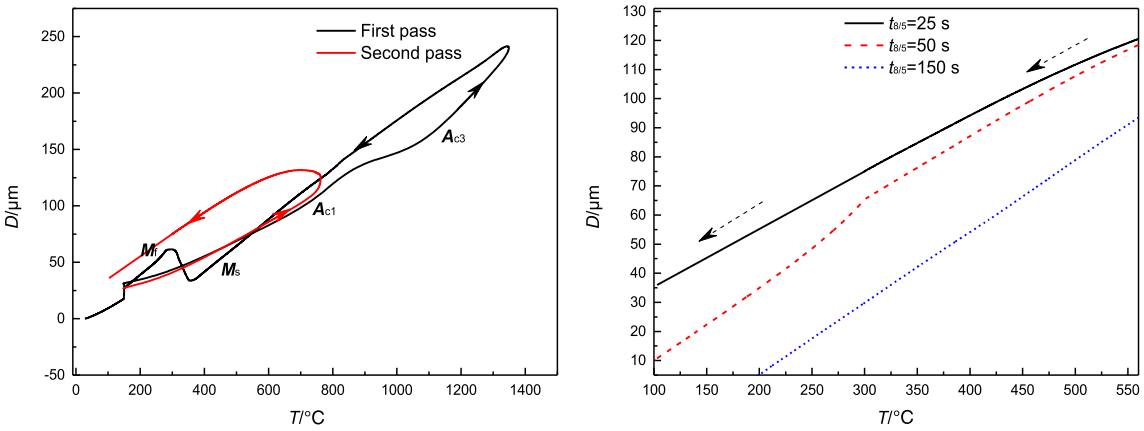

Fig. 10 Dilatation curves in SCGHAZ. **a** $t_{8/5}$ = 25 s–25 s; **b** cooling

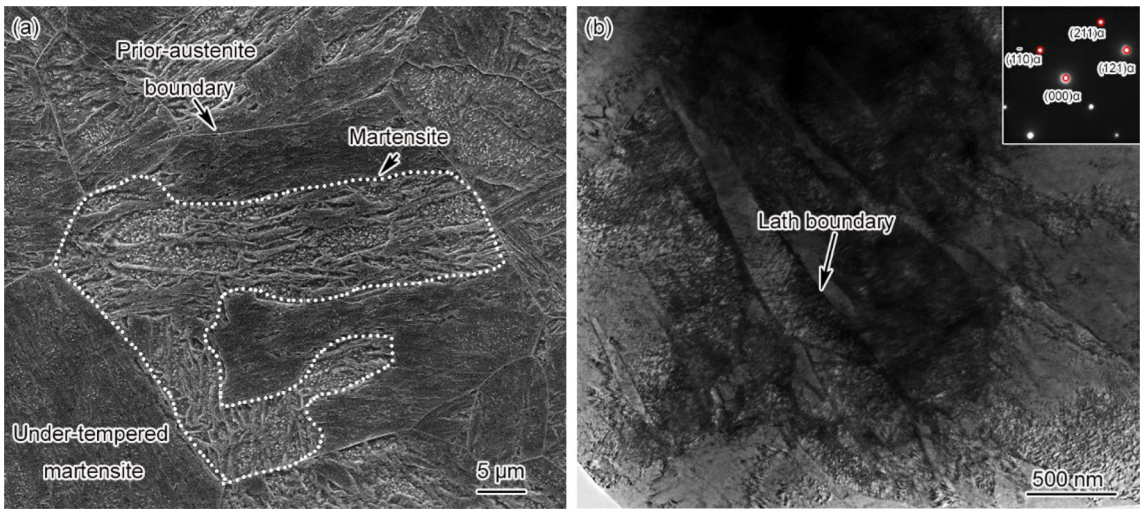

Fig. 11 Microstructure of SCGHAZ, $t_{8/5}$ = 25 s–25 s. **a** SEM; **b** TEM

the martensite region was clear, and numerous dislocation tangles and sub-grains existed (Fig. 11b).

According to Figs. 10 and 11, the phase transformation law of SCCGHAZ in G115 steel welding is defined as:

$$M_{Tempered} \xrightarrow{heating} \gamma_{First} \xrightarrow{cooling} M_{First} \xrightarrow{heating} M_{First} + M_{Under-tempered} \xrightarrow{cooling} M_{First} + M_{Under-tempered}.$$

3.6 Microhardness

The microhardness in the reheated CGHAZ of G115 steel at different $t_{8/5}$ is presented in Fig. 12. The average microhardness of the respective sub-region of the reheated CGHAZ was 443 HV1 (UACGHAZ), 458 HV1 (SCCGHAZ), 327 HV1 (IRCGHAZ) and 423 HV1 (SCGHAZ), respectively. The microhardness of UACGHAZ, SCCGHAZ and SCGHAZ fell to the range of martensite hardness, and the microhardness of IRCGHAZ was lower than that of martensite. The microhardness in the respective sub-region of the reheated CGHAZ decreased with the increase in $t_{8/5}$ except for SCGHAZ, and the microhardness of SCGHAZ first increased and then decreased with the increase in $t_{8/5}$. At the identical $t_{8/5}$ except for $t_{8/5}$ = 25 s, the microhardness first increased, then decreased and subsequently increased again with the decrease in T_{p2} during the second thermal cycle. The peak was detected in SCCGHAZ, and the minimum value appeared in IRCGHAZ; when $t_{8/5}$ = 25 s, the microhardness first decreased and then increased with the decrease in T_{p2} during the second thermal cycle, and the minimum value was detected in IRCGHAZ.

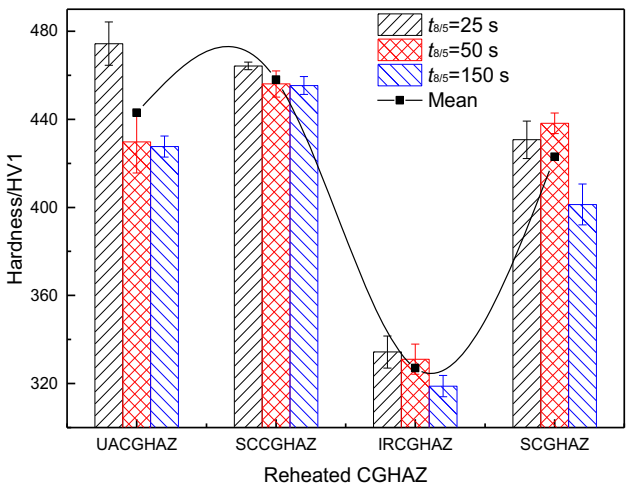

Fig. 12 Microhardness of reheated CGHAZ of G115 steel

4 Discussion

4.1 Microstructure evolution

Microstructure acts as the factor critically determining the properties of materials. The microstructure of materials will be altered in the course of hot working, thereby impacting their properties. Overall, the HAZ turned out to be the weak area of the joint performance after welding of conventional heat-resistant steels. G115 steel, likewise, whose HAZ was another area with largely fluctuated microstructure and properties, which is considered the research hot spot. The microstructure of UACGHAZ, SCCGHAZ and SCGHAZ in the reheated CGHAZ of G115 steel was largely martensite. The dislocation density and the number of sub-grains in the lath were larger, which gradually decreased, and their prominent properties could be ensured during the subsequent service period. The

microstructure of IRCGHAZ was martensite and over-tempered martensite, and there were considerable revival structure and undissolved carbides in the over-tempered martensite region. The dislocation density and the number of sub-grains plummeted. Moreover, a small amount of Laves phase was found. Such complex multiphase structure adversely affected the creep property of the material at high temperatures.

4.2 Effect of welding thermal cycle on A_{c1}, A_{c3}, M_s and M_f

The welding thermal cycle will affect A_{c1} and A_{c3}. According to Fig. 1a, A_{c1} and A_{c3} during the first thermal cycle reached 821 and 1131 °C, respectively, and the austenite transformation took 1.6 s; A_{c1} and A_{c3} during the second thermal cycle are 807 and 1087 °C, respectively, and the austenite transformation took 1.3 s. A_{c1} and A_{c3} during the second thermal cycle were significantly lower than those during the first thermal cycle; such phenomenon remained unchanged with the variation of welding $t_{8/5}$, whereas it was directly associated with the austenite transforming mechanism during the two thermal cycles. The reason why A_{c1} and A_{c3} were higher during the first thermal cycle was that the tempered martensite was transformed to the austenite under the diffusion mechanism, requiring higher temperature and longer holding time. During the second thermal cycle, the martensite (transformed product of the first thermal cycle) was transformed to austenite with the non-diffusion (shear) mechanism, thereby requiring lower temperature and shorter time. The austenite transformation following the non-diffusion (shear) mechanism was directly associated with the original state of the material. Kimmins and Gooch [21] investigated the transforming mechanism of 1Cr–1Mo–0.75V(Ti, B) austenite and reported that when the original structure is martensite and covers a small amount of retained austenite, the austenite transformation is easy to take place with the non-diffusion (shear) mechanism, which is termed as the austenite memory effect. Nakada et al. [22] determined three types of austenite memory effects, i.e., shear recovery mechanism, variation constraint mechanism and retained austenite mechanism. On the whole, the retained austenite maintained a coherent relationship with martensite. When austenite transformation took place, it would be rapidly transformed to austenite with the retained austenite as the center, thereby reducing A_{c1} and A_{c3}. The transformed product of G115 steel after the first thermal cycle was martensite. The retained austenite was distributed between the martensite laths in the form of lamellar, maintaining a coherent relationship with the matrix and satisfying the K–S relationship [23, 24], i.e., $(111)_{\gamma\text{-Fe}}//(110)_{\alpha\text{-Fe}}$ (Fig. 13), effectively underpinning the transformation of martensite into austenite with the shear mechanism during the second thermal cycle. Moreover, it can be inferred that the austenite memory effect during the second thermal cycle of G115 steel can be explained by the mechanism of retained austenite. The memory effect of austenite is easy to occur during multi-layer welding and heat treatment of alloy steel. It is noteworthy that during multi-layer welding, as impacted by the rapid heating rate and high peak temperature, the coarse-grained zone will undergo numerous high-temperature thermal cycles, causing the austenite memory effect and low-temperature martensite transformation repeatedly. For the mentioned effect mechanism, the austenite cannot recrystallize and refine the microstructure, resulting in coarse structure, microhardness increase, brittleness increase and toughness decrease in the reheated CGHAZ. Overall, the harmfulness could be alleviated by postweld heat treatment, whereas it cannot be thoroughly eliminated.

The welding thermal cycle T_p could affect the M_s and M_f of IRCGHAZ. The M_s and M_f of IRCGHAZ during the first thermal cycle were 395 and 275 °C, respectively (Fig. 7a). When $t_{8/5}$ of the second thermal cycle was 25, 50 and 150 s, the corresponding M_s was 395, 415 and 432 °C, respectively, and M_f was 233, 242 and 213 °C, respectively, as shown in Fig. 7b. During the second thermal cycle, except the $t_{8/5}$ = 25 s, M_s was higher than that of the first thermal cycle, and the gap increased with the increase in $t_{8/5}$ of the second thermal cycle. The main factors of M_s are the alloy content and its stability in the austenite [25]. During the second thermal cycle, T_{p2} was between A_{c1} and A_{c3}, and the content and stability in the austenite were significantly less than those of the first thermal cycle, leading to the increase in M_s. Moreover, the formation of carbides and precipitates increased with the increase in $t_{8/5}$, further reducing the alloy content and stability of austenite and resulting in the increase in M_s with the increasing $t_{8/5}$.

4.3 Evolution of precipitate

Due to T_{p1} = 1350 °C during the first thermal cycle, all precipitates in the base metal of G115 steel have been completely dissolved, and there was no precipitate in CGHAZ; for T_{p2} = 1350 °C during the second thermal cycle of UACGHAZ, the precipitates formed would be completely dissolved again, and there was no precipitate; T_{p2} during the second thermal cycle of SCCGHAZ decreases, the precipitates could not be completely dissolved again, and there would be a small quantity of undissolved $M_{23}C_6$ carbides, as shown in Fig. 6; T_{p2} during the second thermal cycle of IRCGHAZ was between A_{c1} and A_{c3}, the number of undissolved carbides would surge, and a small amount of Laves phase appeared, as shown in

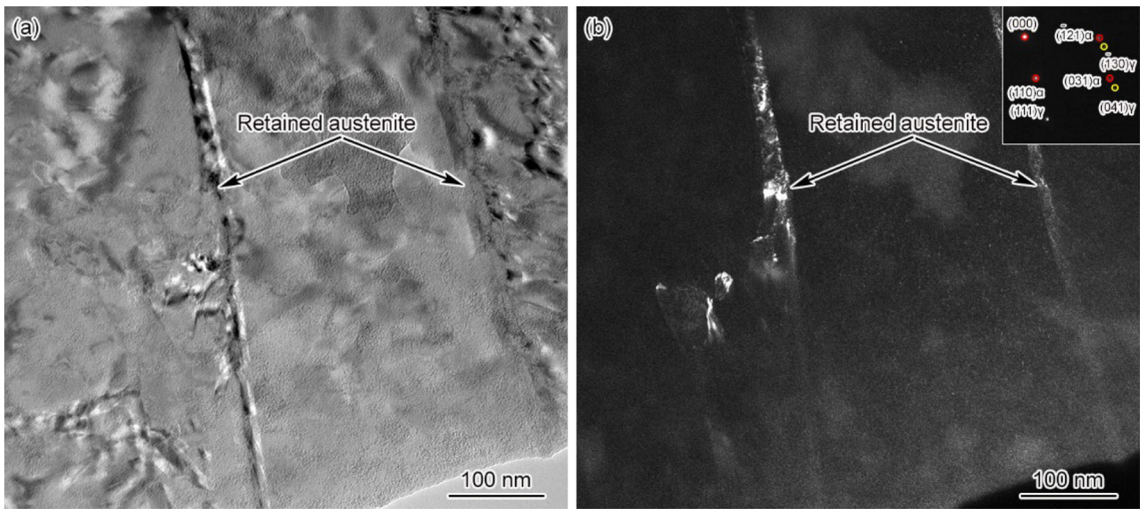

Fig. 13 Retained austenite. **a** Bright field image; **b** dark field image

Fig. 9. T_{p2} during the second thermal cycle of SCGHAZ was lower than A_{c1}, and the under-tempered martensite only underwent recovery without precipitates. Moreover, no MX carbide, μ phase and Cu-rich phase were identified after the analysis of the precipitates in the reheated CGHAZ, indicating that the mentioned precipitates would not be formed in the reheated CGHAZ of G115 steel.

As known from the mentioned analysis, there were precipitates in both SCCGHAZ and IRCGHAZ sub-regions, where the number and type of IRCGHAZ took up the majority. The analysis of IRCGHAZ precipitates indicated that the size of $M_{23}C_6$ in this region was between the base metal and SCCGHAZ. Under the rapid heating during the second thermal cycle, the martensite underwent tempering, and carbides precipitated rapidly. For the short holding time, there was insufficient time for the carbides to grow up, and they remained in the cooling. According to TEM analysis, carbides precipitated by rapid heating could maintain a certain orientation relationship with the matrix, as shown in Fig. 9a. Moreover, a small amount of Laves phase was found in the over-tempered region. According to Refs. [1, 10, 11], the Laves phase was only formed in the case of long-term aging or service, and appearance of the Laves phase mostly indicated that the high-temperature creep strength of the material began to decline. According to Ref. [8], the Laves phase mainly complied with two nucleation mechanisms, i.e., precipitation in the region adjacent to $M_{23}C_6$ and formation on the martensite lath boundary or the original austenite grain boundary. In G115 steel, there was a greater tendency for W to segregation and acting as the main element for the Laves phase formation, effectively underpinning nucleation of the Laves phase. Moreover, the nucleation of Laves phase showed a close relation to the diffusion of Si [26]. The analysis of Laves phase in the over-tempered region of IRCGHAZ demonstrated that there were considerable $M_{23}C_6$ carbides around the phase, and the dislocation density around the phase decreased sharply. Moreover, a small amount of Si was contained in the Laves phase. Compared with the Laves phase in G115 steel during the high-temperature aging, formation of the Laves phase was also accompanied by carbide coarsening [27], dislocation density reduction and microregion recovery. The distribution of these two was significantly similar, indicating that the microstructure and properties of IRCGHAZ over-tempered region of G115 steel were significantly similar to those after aging or service, and it was the area with weak high-temperature creep property in the reheated CGHAZ of G115 steel. According to the thermal equilibrium phase diagram of G115 steel, the Laves phase was only formed in a certain temperature range. As shown in Fig. 14, the Laves phase would not be formed under higher T_{p2} during the second thermal cycle of

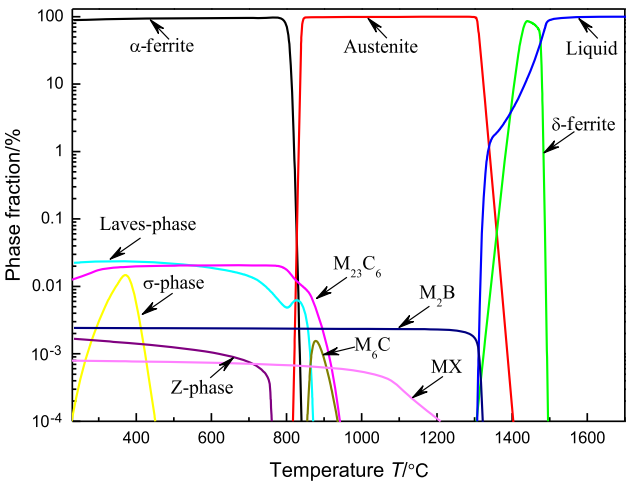

Fig. 14 Calculated equilibrium phase fractions for G115 steel as a function of temperature

UACGHAZ and SCCGHAZ and lower T_{p2} during the second thermal cycle of SCGHAZ.

4.4 Evolution of microhardness

The microstructure, substructure and microhardness of reheated CGHAZ are closely related to the second thermal cycle T_{p2}. With the decrease in T_{p2} during the second thermal cycle, the microstructure is coarse lath martensite (UACGHAZ), lath martensite (SCCGHAZ), lath martensite + over-tempered martensite (IRCGHAZ), lath martensite + under-tempered martensite (SCGHAZ). The lath martensite contains higher dislocation density and more sub-grains due to the rapid shear transformation mechanism from austenite to martensite. Its high microhardness is the main manifestation of dislocation strengthening. The microhardness of martensite is directly associated with not only dislocation density but also the size of martensite block, package and lath. The strength and microhardness increase when the size of martensite block, package and lath is small. Although the microstructures of UACGHAZ and SCCGHAZ are lath martensite, the T_{p2} of UACGHAZ is higher, increasing the size of martensite block, package and lath, and decreasing the microhardness, as illustrated in Figs. 3 and 4. For SCCGHAZ, the T_{p2} is lower, the size of martensite block, package and lath is smaller, and the microhardness is higher compared to UACGHAZ, as presented in Fig. 4. The size of martensite block, package and lath is the main reason for the difference in microhardness between UACGHAZ and SCCGHAZ. The average microhardness difference between them is about 20 HV1.

The microstructure of IRCGHAZ is over-tempered martensite and fresh martensite. The former is because T_{p2} is much higher than the tempering temperature of G115 steel, leading to the formation of high-temperature tempered martensite and over-tempering effect. Its microstructure is characterized by coarse precipitates, sharply decreasing dislocation density and the number of sub-grains, and decreasing strength and microhardness in terms of properties. As mentioned in Ref. [2], the existence of over-tempered martensite in inter-critical heat-affected zone results in softening zone in P91 steel-welded joint. There are softening zones in P91, P92 and G115 steel-welded joints that are all directly related to the formation of over-tempered or over-aged microstructure. Meanwhile, a certain amount of fresh martensite exists in IRCGHAZ with small content and uneven distribution. Therefore, the existence of over-tempered structure is the main reason for the sharp decrease in microhardness of IRCGHAZ, and the uneven distribution of mixed structure is not conducive to the improvement of properties and microhardness. On this basis, IRCGHAZ is the sub-zone with the smallest average microhardness in the reheated CGHAZ.

The microstructure of SCGHAZ consists of martensite and under-tempered martensite. The former maintains a high microhardness, while the latter recovers to a certain extent. The dislocation density, the average microhardness and the number of sub-grains are bound to be lower than those of UACGHAZ and SCCGHAZ.

In the same reheated CGHAZ sub-zone, the increase in $t_{8/5}$ during the second thermal cycle from 25 to 150 s does not change the sub-regional microstructure, but slightly impacts the substructure. The increase in $t_{8/5}$ usually leads to the increase in lath spacing and precipitate size and the decrease in dislocation density and microhardness.

5 Conclusions

1. In the reheated CGHAZ of G115 steel, the microstructure of UACGHAZ and SCCGHAZ is lath martensite, and structural heredity occurs. The microstructure of IRCGHAZ consists of lath martensite and over-tempered martensite, and SCGHAZ covers lath martensite and under-tempered martensite.
2. In UACGHAZ and SCCGHAZ, the austenite is transformed with the diffusion mechanism during the first thermal cycle and with the shear mechanism during the second thermal cycle, thereby resulting in A_{c1} and A_{c3} during the second thermal cycle significantly lower than those during the first thermal cycle. In IRCGHAZ, the content and stability of austenite alloy during the second thermal cycle are lower than those during the first thermal cycle, which leads to the increase in M_s.
3. There are undissolved precipitates in both SCCGHAZ and IRCGHAZ, where the number and type of IRCGHAZ take up the majority. The Laves phase, adversely affecting high-temperature creep property, is identified in the over-tempered region.
4. IRCGHAZ exhibits over-tempered martensite, lower dislocation density and the number of sub-grains, thereby resulting in the sharp decrease in microhardness. It is the weak area of the reheated CGHAZ of G115 steel.

Acknowledgements We would like to acknowledge the support of National Key R&D Program of China (No. 2017YFB0305202), Inner Mongolia Natural Science Foundation (No. 2016MS0510), and Inner Mongolia Natural Science Foundation (No. 2020MS05046).

References

[1] Z.D. Liu, Z.Z. Chen, X.K. He, H.S. Bao, Acta Metall. Sin. (Engl. Lett.) 56 (2020) 539–548.
[2] M. Sireesha, S. Sundaresan, S.K. Albert, J. Mater. Eng. Perform. 10 (2001) 320–330.
[3] J. Klöwer, R.U. Husemann, M. Bader, Proced. Eng. 55 (2013) 226–231.
[4] P. Yan, Z.D. Liu, H.S. Bao, Y.Q. Weng, W. Liu, Mater. Sci. Eng. A 597 (2014) 148–156.
[5] P. Yan, Z.D. Liu, H.S. Bao, Y.Q. Weng, W. Liu, Mater. Des. 54 (2014) 874–879.
[6] P. Yan, Z.D. Liu, Mater. Sci. Eng. A 650 (2016) 290–294.
[7] L.Y. Xu, J.Y. Rong, L. Zhao, H.Y. Jing, Y.D. Han, Mater. Sci. Eng. A 726 (2018) 179–186.
[8] B. Xiao, L.Y. Xu, Z.X. Tang, L. Zhao, H.Y. Jing, Y.D. Han, H.Z. Li, Mater. Sci. Eng. A 747 (2019) 161–176.
[9] Z. Liu, Z.D. Liu, X.T. Wang, Z.Z. Chen, L.T. Ma, Mater. Sci. Eng. A 729 (2018) 161–169.
[10] F. Abe, M. Tabuchi, S. Tsukamoto, T. Shirane, Int. J. Pres. Ves. Pip. 87 (2010) 598–604.
[11] S.K. Albert, M. Matsui, T. Watanabe, H. Hongo, K. Kubo, M. Tabuchi, Int. J. Pres. Ves. Pip. 80 (2003) 405–413.
[12] T. Matsunaga, H. Hongo, M. Tabuchi, R. Sahara, Mater. Sci. Eng. A 655 (2016) 168–174.
[13] K.G. Abstoss, S. Schmigalla, S. Schultze, P. Mayr, Mater. Sci. Eng. A 743 (2019) 233–242.
[14] W.B. Gao, D.P. Wang, F.J. Cheng, X.J. Di, C.Y. Deng, W. Xu, J. Mater. Process. Technol. 238 (2016) 333–340.
[15] K. Peng, C.L. Yang, S.B. Lin, C.L. Fan, Int. J. Adv. Manuf. Technol. 90 (2017) 3387–3395.
[16] K.S. Arora, S.R. Pandu, N. Shajan, P. Pathak, M. Shome, Int. J. Pres. Ves. Pip. 163 (2018) 36–44.
[17] X. Wang, J.W. Chang, G.Z. Huang, Y.L. Zhang, Trans. China Weld. Inst. 29 (2008) No. 10, 29–32+114.
[18] X. Wang, J.W. Chang, F.Y. Chen, M.L. Qiu, Trans. China Weld. Inst. 29 (2008) No. 3, 9–12+153.
[19] X. Xu, G.D. West, J.A Siefert, J.D. Parker, R.C. Thomson, Metall. Mater. Trans. A 49 (2018) 1211–1230.
[20] Y. Liu, S. Tsukamoto, K. Sawada, M. Tabuchi, F. Abe, Metall. Mater. Trans. A 46 (2015) 1843–1854.
[21] S.T. Kimmins, D.J. Gooch, Met. Sci. 17 (1983) 519–532.
[22] N. Nakada, T. Tsuchiyama, S. Takaki, S. Hashizume, ISIJ Int. 47 (2007) 1527–1532.
[23] T.Y. Hsu (Z.Y. Xu), Y.W. Mou, Acta Metall. 32 (1984) 1469–1481.
[24] W. Klement Jr., A. Jayaraman, Prog. Solid State Chem. 3 (1967) 289–298.
[25] F.C. Zhang, T.Q. Lei, Wear 212 (1997) 195–198.
[26] A. Aghajani, F. Richter, C. Somsen, S.G. Fries, I. Steinbach, G. Eggeler, Scripta Mater. 61 (2009) 1068–1071.
[27] Y.T. Xu, M.J. Wang, Y. Wang, T. Gu, L. Chen, X. Zhou, Q. Ma, Y.M. Liu, J. Huang, J. Alloy. Compd. 621 (2015) 93–98.